Space-Time Adaptive Linearly Implicit Peer Methods for Parabolic Problems

Dirk Schröder[1], **Alf Gerisch**[1] **and Jens Lang**[1,2]

[1]Department of Mathematics, Technische Universität Darmstadt, Dolivostr. 15, D-64293 Darmstadt, Germany
[2]Graduate School CE, Technische Universität Darmstadt, Dolivostr. 15, D-64293 Darmstadt, Germany.

TECHNISCHE UNIVERSITÄT DARMSTADT

Numerical Analysis

Space-Time Adaptive Linearly Implicit Peer Methods for Parabolic Problems

Dirk Schröder[a,*], Alf Gerisch[a], Jens Lang[a,b]

[a] *Department of Mathematics, Technische Universität Darmstadt, Dolivostraße 15, 64293 Darmstadt, Germany*
[b] *Graduate School of Computational Engineering, TU Darmstadt*

Abstract

In this paper a linearly implicit peer method is combined with a multilevel finite element method for the discretization of parabolic partial differential equations. Following the Rothe method it is first discretized in time and then in space. A spatial error estimator based on the hierarchical basis approach is derived. It is shown to be a reliable and efficient estimator up to some small perturbations. The efficiency index of the estimator is shown to be close to the ideal value one for some one-dimensional test problems. Finally we compare the performance of the overall method, based on second, third, and fourth order peer methods with that of some Rosenbrock methods. We conclude that the presented peer methods offer an attractive alternative to Rosenbrock methods in this context.

Keywords: finite elements, linearly implicit peer methods, adaptivity, Rothe method

1. Introduction/Motivation

In [1] linearly implicit peer methods were introduced for the numerical solution of time-dependent PDEs. The authors followed the Rothe approach, discretizing first in time with a linearly implicit peer method and then solving the arising linear elliptic problems with the finite element method. This approach was already shown to be efficient for Rosenbrock methods [2]. The combination of peer methods with finite elements was implemented and tested within the software package *KARDOS* [3].

The main advantage of peer methods is that they do not show order reduction when applied to stiff ODEs or PDEs [4], as it is the case for Rosenbrock methods [5]. Furthermore, peer methods have good stability properties in comparison with other multistep methods. There are $A(\alpha)$-stable methods available with an α almost equal 90 degrees.

However, the presented method in [1] is only adaptive in time and fixed spatial grids are used for the whole integration. Many problems like the prop-

*Corresponding author
Email addresses: schroeder@mathematik.tu-darmstadt.de (Dirk Schröder), gerisch@mathematik.tu-darmstadt.de (Alf Gerisch), lang@mathematik.tu-darmstadt.de (Jens Lang)

agation of a flame front are solved more efficiently using also adaptive spatial grids. In this paper we want to fill this gap.

We combine the linearly implicit peer method within the Rothe approach with a multilevel finite element method. Thus we do not use a fixed spatial grid but we build a sequence of nested finite element spaces at every time step. The nested spaces are constructed adaptively with respect to a local spatial error estimation based on a hierarchical basis.

The paper is organized as follows. In section 2 we specify the problem setting. Then we give a short overview to linearly implicit peer methods and the used time error estimation. In section 4 we present the finite element solution of the arising linear elliptic equations and derive the spatial error estimator. The error estimator is then proven to be efficient and robust up to some small perturbations. In section 5 we present some numerical experiments in one spatial dimension concerning the efficiency of the spatial error estimation. The performance of the presented method is then compared to Rosenbrock methods for some test problems in two spatial dimensions in section 6. Finally our results are summarized.

2. Parabolic Partial Differential Equations

We consider the nonlinear initial boundary value problem

$$\begin{aligned} \partial_t y(x,t) &= f(x,t,y(x,t)) && \text{in } \Omega \times (0,T], \\ B(x,t,y(x,t))y(x,t) &= g(x,t,y(x,t)) && \text{on } \partial\Omega \times (0,T], \\ y(x,0) &= y_0(x) && \text{on } \bar{\Omega}. \end{aligned} \tag{1}$$

in the same setting as in [6] and [2]. $\Omega \subset \mathbb{R}^d, d = 1, 2$ or 3, denotes a bounded domain with sufficiently smooth boundary $\partial\Omega$. f is a partial differential operator. The boundary operator B stands for a system of boundary conditions interpreted in the sense of traces. g is a given function and y_0 is the initial condition.

We consider a Gelfand triple of separable Hilbert spaces $\mathcal{V}$, $\mathcal{H}$ and $\mathcal{V}'$ with $\mathcal{V} \overset{ds}{\hookrightarrow} \mathcal{H} \overset{ds}{\hookrightarrow} \mathcal{V}'$. We denote the norm on $\mathcal{H}$ induced by the scalar product $(\cdot,\cdot)$ with $|\cdot|$, the norm on $\mathcal{V}$ induced by the scalar product $((\cdot,\cdot))$ with $||\cdot||$, and the dual norm on $\mathcal{V}'$ by $||\cdot||_*$. The anti duality between $\mathcal{V}$ and $\mathcal{V}'$ is denoted by $\langle\cdot,\cdot\rangle$.

With the operator $F : (0,T] \times \mathcal{V} \to \mathcal{V}'$ we rewrite (1) as an abstract Cauchy problem of the form

$$\partial_t y(t) = F(t, y(t)), \quad 0 < t \leq T, \quad y(0) = y_0. \tag{2}$$

We assume that (2) has a unique, temporally smooth solution $y(t)$.

We suppose that F is sufficiently differentiable. We set

$$A(t,w) := -F_y(t,w). \tag{3}$$

We assume that $A(t,w) : \mathcal{V} \to \mathcal{V}'$ is a sectorial operator for $t \in (0,T]$ and $w \in \mathcal{W} \subset \mathcal{V}$. The operator $A(t,w)$ is associated with a sesquilinear form

$$a(t,w;v_1,v_2) = \langle A(t,w)v_1, v_2\rangle, \quad v_1, v_2 \in \mathcal{V}. \tag{4}$$

We assume that for all $w \in \mathcal{W}$ and $t \in [0,T]$ the sesquilinear form $a(t,w;v_1,v_2)$ is continuous

$$|a(t,w;v_1,v_2)| \leq M_a||v_1||||v_2|| \quad \forall v_1,v_2 \in \mathcal{V} \tag{5}$$

and $\mathcal{V}$-elliptic

$$a(t,w;v_1,v_1) \geq \mu_a||v_1||^2, \quad \forall v_1 \in \mathcal{V}, \tag{6}$$

with constants M_a and μ_a independent of $t \geq 0, w, v_1$ and v_2. Furthermore, we require Lipschitz continuity of $t \mapsto A(t,w(t))$ in the $\mathcal{L}(\mathcal{V},\mathcal{V}')$-norm, i.e.

$$||A(t_2,w(t_2)) - A(t_1,w(t_1))||_{\mathcal{L}(\mathcal{V},\mathcal{V}')} \leq L|t_2 - t_1|, \quad \forall t_1,t_2 \in [0,T]. \tag{7}$$

Also we assume for the regularity of the second derivatives of F:

$$||F_{ty}(t,v)v_1||_* \leq C_1||v_1|| \qquad \forall v_1 \in \mathcal{V}, \tag{8}$$

$$||F_{yy}(t,v)[v_1,v_2]||_* \leq C_2||v_1||||v_2|| \qquad \forall v_1,v_2 \in \mathcal{V}, \tag{9}$$

with C_1, C_2 independent of v varying in bounded subsets of $\mathcal{V}$ and $t \in [0,T]$.

By setting $Q(t,v) = F(t,v) + A(t,v)v$ for all $v \in \mathcal{V}$, we can rewrite (2) in the form of a quasilinear Cauchy problem

$$\partial_t y + A(t,y)y = Q(t,y), \quad 0 < t \leq T, \quad y(0) = y_0. \tag{10}$$

From continuity (5) we deduce that $A(t,v)$ is uniformly bounded and has a uniformly bounded inverse A^{-1} [2]. Furthermore, $\mathcal{V}$-ellipticity (6) implies the existence of constants $M > 0$ and angle $\phi < \frac{\pi}{2}$ such that the resolvent bound

$$||(\lambda I + A(t,w))^{-1}||_{\mathcal{L}(\mathcal{V})} \leq \frac{M}{1+|\lambda|}$$

holds for all $w \in \mathcal{W}$ and for all $\lambda \in \mathbb{C}$ with $|\arg(\lambda)| \leq \pi - \phi$ [2]. This setting is the usual one for differential equations of parabolic type and includes the case of semilinear and quasilinear parabolic equations in two and three space dimensions [6].

3. Linearly Implicit Peer Methods

Let τ_n be the step size at time step $n \geq 1$. An s-stage linearly implicit peer method [1] computes approximations $Y_{ni} \in \mathcal{V}$, $i = 1,\ldots,s$, to the exact solution of (2) at time points $t = t_{ni}$, i.e., $Y_{ni} \approx y(t_{ni})$, by

$$(I - \tau_n\gamma J_n)\,(Y_{ni} - Y_{ni}^0) = \tau_n\gamma F(t_{ni},Y_{ni}^0) + w_{ni} - Y_{ni}^0, \tag{11a}$$

$$Y_{ni}^0 = \sum_{j=1}^{i-1} \frac{1}{\gamma} a_{ij}^0 (Y_{nj} - w_{nj}) + \sum_{j=1}^{s} u_{ij}^0(\sigma_n) Y_{n-1,j}, \tag{11b}$$

$$w_{ni} = \sum_{j=1}^{i-1} \frac{1}{\gamma} a_{ij} (Y_{nj} - w_{nj}) + \sum_{j=1}^{s} u_{ij}(\sigma_n) Y_{n-1,j}. \tag{11c}$$

The predictor values Y_{ni}^0 are also approximations to the exact solution of (2) at time points t_{ni}. The step size ratio is denoted by $\sigma_n := \tau_n/\tau_{n-1}$. The coefficients of the method are collected in the full matrix $U(\sigma) = (u_{ij}(\sigma))_{i,j=1}^s \in \mathbb{R}^{s\times s}$ and

the lower triangular matrix $A = (a_{ij})_{i,j=1}^{s} \in \mathbb{R}^{s\times s}$. Since we consider only singly implicit methods, we have $a_{ii} = \gamma$ for all $i = 1, \ldots, s$ for some $\gamma \in \mathbb{R}$.

The matrices $A^0 = (a^0_{ij})$ and $U^0 = (u^0_{ij})$ are $s \times s$ real-coefficient matrices for the predictor Y^0_{ni}. A^0 is strictly lower triangular and U^0 depends again on the step size ratio σ_n. For details on their construction, we refer to [1]. The vector $c = (c_i) \in \mathbb{R}^s$ denotes the vector of pairwise distinct abscissae of the method. We set $c_s = 1$. The time points t_{ni} are then defined by $t_{ni} := t_n + c_i\tau_n$ for $n = 1, 2, \ldots$, and $i = 1, \ldots, s$ and especially $t_n := t_{n-1,s}$. There are no further restrictions on the values c_i. The matrix J_n is an approximation to the Jacobian of F at $(t_n, Y_{n-1,s})$. We only assume that there is a $\omega_n \in \mathcal{W}$ such that

$$J_n = F_y(t_n, \omega_n).$$

Note that J_n is constant for each time step.

Different choices of the c_i have been considered in the literature. In [1] and [7] the values are chosen as the stretched Chebychev nodes

$$c_i := -\frac{\cos((i - \frac{1}{2})\frac{\pi}{s})}{\cos(\frac{\pi}{2s})}, \quad i = 1, 2, \ldots, s,$$

lying in the interval $[-1, 1]$. The reason of this choice is the small condition number of the corresponding Vandermonde matrix, which avoids inaccuracies in the computation of the method coefficients. In [8] the abscissae are restricted to the interval $(0, 1]$, which corresponds to the range used in classical methods of advancing forward in time and makes a dense output available.

In this paper we will use a second, third, and fourth order method with strictly positive nodes c_i, based on the coefficients presented in [8], which we will refer to as *peer3pos*, *peer4pos*, and *peer5pos*, respectively. Since strictly positive nodes allow for a dense output, they are advantageous in the context of optimal control. The overall performance is similar to other peer methods presented in [1] and [7]. Therefore, we decided to only present numerical results for the peer methods with positive nodes.

Remark 3.1. In [1] it is remarked, that by solving the recursions (11b) and (11c) for Y^0_{ni} and w_{ni}, we get the following equivalent computation formula

$$w_{ni} = \sum_{j=1}^{i-1} \bar{a}_{ij} Y_{nj} + \sum_{j=1}^{s} \bar{u}_{ij}(\sigma_n) Y_{n-1,j}, \tag{12}$$

$$Y^0_{ni} = \sum_{j=1}^{i-1} \bar{a}^0_{ij} Y_{nj} + \sum_{j=1}^{s} \bar{u}^0_{ij}(\sigma_n) Y_{n-1,j}, \tag{13}$$

with coefficients $\bar{A} := I - \gamma A^{-1}$, $\bar{U}(\sigma_n) := \gamma A^{-1} U(\sigma_n)$, $\bar{A}^0 := I - \gamma (A^0)^{-1}$ and $\bar{U}^0(\sigma_n) := \gamma (A^0)^{-1} U^0(\sigma_n)$. In this form only the approximations $Y_{n,j}$, $Y_{n-1,j}$, $j = 1, \ldots, s$, and the value w_{ni} of the current stage need to be stored within time step n. □

If the predictor has order $p = s - 1$ and the coefficients U and A fulfill the order conditions for an implicit peer method [8] of order $p = s - 1$, then the resulting linearly implicit peer method has also order $p = s-1$ [1]. Furthermore, since the linearly implicit peer method is equivalent to the implicit peer method for linear problems, both have the same linear stability properties [1].

The starting values $Y_{0i} \approx y(t_1 + (c_i - 1)\tau_0)$ are computed by a Rosenbrock method of corresponding order, cf. [1].

4. Solving the spatial problems

To solve the PDE system (2), we follow the Rothe approach, that is, we first discretize in time and then in space. Discretizing in time with a linearly implicit peer method (11) leads to the following system:

$$Y_{ni} - Y_{ni}^0 - \tau_n \gamma J_n (Y_{ni} - Y_{ni}^0) = \tau_n \gamma F(t_{ni}, Y_{ni}^0) + w_{ni} - Y_{ni}^0, \quad 1 \le i \le s. \tag{14}$$

Equation (14) is a system of linear elliptic equations. The linearity of the resulting elliptic systems is in fact the major motivation to use linearly implicit integration schemes. To solve the linear elliptic problems, we use a multilevel finite element method [2].

Following the Galerkin approach, the weak formulation of (14) is given by

$$\begin{aligned} \forall \varphi \in \mathcal{V}: \quad \langle Y_{ni} - Y_{ni}^0, \varphi \rangle - \tau_n \gamma \langle J_n (Y_{ni} - Y_{ni}^0), \varphi \rangle = \\ \langle \tau_n \gamma F(t_{ni}, Y_{ni}^0) + w_{ni} - Y_{ni}^0, \varphi \rangle, \quad 1 \le i \le s. \end{aligned} \tag{15}$$

Here, φ are the test functions taken from $\mathcal{V}$. Note that since $\mathcal{V}$ is continuously embedded in its dual space $\mathcal{V}'$, we can identify $v \in \mathcal{V}$ as an element in $\mathcal{V}'$. We introduce the stage update $Y_{ni}^U = Y_{ni} - Y_{ni}^0$ and the sesquilinear form

$$b_n(v_1, v_2) := \langle v_1, v_2 \rangle + \tau_n \gamma a(t_n, \omega_n; v_1, v_2), \quad v_1, v_2 \in \mathcal{V}.$$

Then we rewrite the weak formulation (15) in the following way:

$$\begin{aligned} \forall \varphi \in \mathcal{V}: \quad b_n(Y_{ni}^U, \varphi) = & \langle \tau_n \gamma F(t_{ni}, Y_{ni}^0) + w_{ni} - Y_{ni}^0, \varphi \rangle, \\ Y_{ni} = & Y_{ni}^0 + Y_{ni}^U, \quad 1 \le i \le s. \end{aligned} \tag{16}$$

For the following analysis, we introduce a τ-dependent error norm defined by

$$||v||_\tau^2 := \tau ||v||^2 + |v|^2, \quad v \in \mathcal{V} \tag{17}$$

and the associated sesquilinear form

$$a_\tau(v_1, v_2) = \tau((v_1, v_2)) + (v_1, v_2), \quad v_1, v_2 \in \mathcal{V}. \tag{18}$$

The system (16) is uniquely solvable by the Lax-Milgram Lemma, if the sesquilinear form $b_n(\cdot, \cdot)$ is bounded and elliptic. These conditions are satisfied according to the following Lemma cited from [2].

Lemma 4.1. *Assume that the sesquilinear form $a(\cdot, \cdot)$, defined in (4), satisfies (5) and (6) with constants M_a and μ_a, respectively. Then there exist positive constants M_b and μ_b independent of τ_n such that for all functions $v_1, v_2 \in \mathcal{V}$:*

$$|b_n(v_1, v_2)| \le M_b ||v_1||_\tau ||v_2||_\tau, \tag{19}$$

$$b_n(v_1, v_1) \ge \mu_b ||v_1||_\tau^2. \tag{20}$$

The constants are given by $M_b = \max(1, \gamma M_a)$ and $\mu_a = \min(1, \gamma \mu_a)$.

The idea of finite elements is to approximate the infinite dimensional solution space $\mathcal{V}$ by a finite dimensional subspace $\mathcal{V}_h$. Multilevel finite elements provide a sequence of nested finite element spaces

$$\mathcal{V}_h^{(0)} \subset \mathcal{V}_h^{(1)} \subset \cdots \subset \mathcal{V}_h^{(m)}$$

based on a sequence of increasingly adapted spatial meshes

$$\mathfrak{T}^{(0)} \subset \mathfrak{T}^{(1)} \subset \cdots \subset \mathfrak{T}^{(m)}.$$

We only consider triangulations of Ω as meshes. In our case the multilevel process stops if a scalar estimate ϵ_{ns}^h of the error $Y_{ns} - Y_{ns}^{h,(m)}$, where $Y_{ns}^{h,(m)}$ solves (21), see below, with $\mathcal{V}_h = \mathcal{V}_h^{(m)}$, is smaller than a given tolerance TOL_x, i.e.,

$$\epsilon_{ns}^h \leq TOL_x.$$

Remark 4.1. Note that we apply the multilevel process to the whole system (15) at once and not individually for each Y_{ni}, i.e., all stages in one time step are computed on the same mesh. Hence, at every time step we have to manage only two different meshes: the actual one and the mesh of the previous time step. □

4.1. Discretization of the stage problems

Given a mesh $\mathfrak{T}$ and the approximations of the previous time step, $Y_{n-1,i} \in \mathcal{V}_{h,prev}$, $i = 1, \ldots, s$, on the mesh $\mathfrak{T}_{prev}$, we want to solve (16) on a finite dimensional subspace $\mathcal{V}_h(\mathfrak{T})$ of $\mathcal{V}$. Replacing $\mathcal{V}$ by the FE space $\mathcal{V}_h$ in (16) gives the following finite dimensional system to compute $Y_{ni}^{h,U} \in \mathcal{V}_h$:

$$\begin{aligned}
\forall \varphi \in \mathcal{V}_h: \quad b_n(Y_{ni}^{h,U}, \varphi) =& \langle \tau_n \gamma F(t_{ni}, Y_{ni}^{h,0}) + w_{ni}^h - Y_{ni}^{h,0}, \varphi \rangle, \\
w_{ni}^h =& \sum_{j=1}^{i-1} \bar{a}_{ij} Y_{nj}^h + \sum_{j=1}^{s} \bar{u}_{ij}(\sigma_n) Y_{n-1,j}^h, \\
Y_{ni}^{h,0} =& \sum_{j=1}^{i-1} \bar{a}_{ij}^0 Y_{nj}^h + \sum_{j=1}^{s} \bar{u}_{ij}^0(\sigma_n) Y_{n-1,j}^h, \\
Y_{ni}^h =& Y_{ni}^{h,0} + Y_{ni}^{h,U}, \quad 1 \leq i \leq s.
\end{aligned} \tag{21}$$

To compute the predictor $Y_{ni}^{h,0}$ and w_{ni}^h, the old stage values $Y_{n-1,i} \in \mathcal{V}_{h,prev}$, $i = 1, \ldots, s$, on the previous mesh $\mathfrak{T}_{prev}$ have to be projected to $Y_{n-1,i}^h \in \mathcal{V}_h$ on the current mesh $\mathfrak{T}$. For this projection we use a C^1 interpolation based on the idea of Lawson [9]. The C^1 interpolation gives smoother numerical solutions than for example an L_2-projection and improves the performance of our adaptive solution process. It was already observed in the context of BDF methods in [10] that smoother numerical solutions benefit multistep methods.

We choose the ansatz space $\mathcal{V}_h(\mathfrak{T})$ as the space of continuous, piecewise linear functions,

$$\mathcal{V}_h(\mathfrak{T}) = \{v \in C(\Omega) : v|_T \in \mathbb{P}_1 \, \forall T \in \mathfrak{T}\} \subset \mathcal{V}.$$

Let $\{\psi_j(x) : j \in \mathcal{J}\}$ be a set of corresponding finite element basis functions on the mesh $\mathfrak{T}$ with the corresponding index set $\mathcal{J}$. The finite element solution Y_{ni}^h can then be written as

$$Y_{ni}^h(x) = \sum_{j \in \mathcal{J}} y_{ni}^{h,j} \psi_j(x).$$

We collect the coefficients $y_{ni}^{h,j}$ into the vector $\mathbf{Y}_{ni}^h$. Similarly we introduce $\mathbf{Y}_{ni}^{h,0}$, $\mathbf{Y}_{ni}^{h,U}$, and $\mathbf{W}_{ni}^h$ for the predictor $Y_{ni}^{h,0}$, the update $Y_{ni}^{h,U}$, and w_{ni}^h, respectively.

Finally the coefficients of the projected old stage value $Y^h_{n-1,i}$ are denoted by $\mathbf{Y}^h_{n-1,i}$.

Inserting the finite element representations in (21), using linearity, and combining the equations for all basis functions ψ_l, $l \in \mathcal{J}$, yields the following linear system

$$\begin{aligned}
(\mathcal{M} + \tau_n\gamma\mathcal{S})\,\mathbf{Y}^{h,U}_{ni} =& \tau_n\gamma\mathcal{F}_i + \mathcal{M}(\mathbf{W}^h_{ni} - \mathbf{Y}^{h,0}_{ni}),\\
\mathbf{W}^h_{ni} =& \sum_{j=1}^{i-1} \bar{a}_{ij}\mathbf{Y}^h_{nj} + \sum_{j=1}^{s} \bar{u}_{ij}(\sigma_n)\mathbf{Y}^h_{n-1,j},\\
\mathbf{Y}^{h,0}_{ni} =& \sum_{j=1}^{i-1} \bar{a}^0_{ij}\mathbf{Y}^h_{nj} + \sum_{j=1}^{s} \bar{u}^0_{ij}(\sigma_n)\mathbf{Y}^h_{n-1,j},\\
\mathbf{Y}^h_{ni} =& \mathbf{Y}^{h,0}_{ni} + \mathbf{Y}^{h,U}_{ni}, \quad 1 \le i \le s,
\end{aligned} \tag{22}$$

with

$$\mathcal{M}_{ij} = \langle\varphi_i, \varphi_j\rangle,\ \mathcal{S}_{ij} = a(\varphi_i, \varphi_j) \text{ and } \mathcal{F}_{i,j} = \langle F(t_{ni}, Y^{h,0}_{ni}), \varphi_j\rangle,\ 1 \le i, j \le s.$$

The matrix $\mathcal{M}$ is the mass matrix, the matrix $\mathcal{S}$ is the stiffness matrix and $\mathcal{F}_i$ is the load vector of the finite element approximation. The mass matrix and the stiffness matrix are assembled only once per mesh. If using direct methods to solve the linear system in (22), the matrix factorization of the left hand side has to be computed only once and then can be used for all stages. The load vector changes in every stage and thus has to be computed for each i.

Finally the coefficients of the predictor are updated with the computed coefficients of the stage update to yield coefficients of the approximation Y^h_{ni} on the finite element mesh $\mathfrak{T}$, that is, $\mathbf{Y}^h_{ni} = \mathbf{Y}^{h,0}_{ni} + \mathbf{Y}^{h,U}_{ni}$. This is equivalent to $Y^h_{ni}(x) = Y^{h,0}_{ni}(x) + Y^{h,U}_{ni}(x)$ for all $x \in \Omega$.

4.2. Estimating the spatial error

To estimate the error of our FE solution Y^h_{ni}, we use the hierarchical basis technique presented for elliptic problems in [11]. The technique was used for the arising linear elliptic systems within a Rothe approach using Rosenbrock methods in [2]. In this section, we will adapt the results for Rosenbrock methods to linearly implicit peer methods.

To this aim, we consider the hierarchical composition

$$\mathcal{V}^+_h = \mathcal{V}_h \oplus \mathcal{V}^\oplus_h \subset \mathcal{V}.$$

The extension space $\mathcal{V}^\oplus_h$ is built by all basis function which are needed to enrich our base space $\mathcal{V}_h$ to the extended space $\mathcal{V}^+_h$ of higher order. We can compute a solution $Y^{h,+}_{ni} \in \mathcal{V}^+_h$ by solving

$$\begin{aligned}
\forall\varphi \in \mathcal{V}^+_h:\quad b_n(Y^{h,U,+}_{ni}, \varphi) =& \langle\tau_n\gamma F(t_{ni}, Y^{h,0,+}_{ni}) + w^{h,+}_{ni} - Y^{h,0,+}_{ni}, \varphi\rangle,\\
w^{h,+}_{ni} =& \sum_{j=1}^{i-1} \bar{a}_{ij}Y^{h,+}_{nj} + \sum_{j=1}^{s} \bar{u}_{ij}(\sigma_n)Y^{h,+}_{n-1,j},\\
Y^{h,0,+}_{ni} =& \sum_{j=1}^{i-1} \bar{a}^0_{ij}Y^{h,+}_{nj} + \sum_{j=1}^{s} \bar{u}^0_{ij}(\sigma_n)Y^{h,+}_{n-1,j},\\
Y^{h,+}_{ni} =& Y^{h,0,+}_{ni} + Y^{h,U,+}_{ni}, \quad 1 \le i \le s.
\end{aligned} \tag{23}$$

Here, $Y^{h,+}_{n-1,i}$ denotes the projection of the old stage value $Y_{n-1,i} \in \mathcal{V}_{h,prev}$ to the extended space $\mathcal{V}^+_h$ for $i = 1, \ldots, s$.

We define the error $E^h_{ni} \in \mathcal{V}$ of the finite element solution at time point t_{ni} as $E^h_{ni} = Y_{ni} - Y^h_{ni}$. Furthermore, we denote the difference between the solution in the base space to the solution in the extended space by $E^{h,+}_{ni} = Y^{h,+}_{ni} - Y^h_{ni} \in \mathcal{V}^+_h$.

In order to show that $E^{h,+}_{ni}$ is an efficient and reliable approximation to E^h_{ni}, we make use of the saturation assumption.

Assumption 4.1 (Saturation Assumption)**.** There exists a constant $\beta < 1$, such that

$$||Y_{ni} - Y^{h,+}_{ni}||_\tau \leq \beta ||Y_{ni} - Y^h_{ni}||_\tau.$$

The saturation assumption is not valid in all cases. Just think of a right-hand side F, such that $Y^{h,+}_{ni} = Y^h_{ni}$. However, for fixed and sufficiently smooth right hand sides the saturation assumption is fulfilled for sufficiently fine meshes [12]. Furthermore, the saturation assumption holds for the extension of linear elements with quadratic elements, if the data oscillation of F is small [13].

The saturation assumption and the triangle inequality imply

$$\frac{1}{1+\beta}||E^{h,+}_{ni}||_\tau \leq ||E^h_{ni}||_\tau \leq \frac{1}{1-\beta}||E^{h,+}_{ni}||_\tau, \tag{24}$$

i.e., $||E^{h,+}_{ni}||_\tau$ is an efficient and reliable error estimator.

4.2.1. Approximation of the spatial error estimator

For ease of notation, we define for vectors $y = (y_1, \ldots, y_s)^T$ and $z = (z_1, \ldots, z_s)^T$ the function

$$\begin{aligned} r_{ni}(y,z) =& \tau_n \gamma F \left(t_{ni}, \sum_{j=1}^{s} \bar{u}^0_{ij}(\sigma_n) y_j + \sum_{j=1}^{i-1} \bar{a}^0_{ij} z_j \right) \\ &+ \sum_{j=1}^{s} (\bar{u}_{ij}(\sigma_n) - \bar{u}^0_{ij}(\sigma_n)) y_j + \sum_{j=1}^{i-1} (\bar{a}_{ij} - \bar{a}^0_{ij}) z_j. \end{aligned} \tag{25}$$

Also we denote, for example, the collection of all stage values in one big vector by

$$Y^h_n := \left(Y^h_{n1}, \ldots, Y^h_{ns}\right)^T \in (\mathcal{V}_h)^s.$$

With these definitions, applying the sesquilinear form $b_n(\cdot,\cdot)$ to $E^{h,+}_{ni}$ gives the following system for the spatial error estimator:

$$\begin{aligned} &\forall \varphi \in \mathcal{V}^+_h : \\ b_n(E^{h,+}_{ni}, \varphi) =& b_n(Y^{h,0,+}_{ni} - Y^{h,0}_{ni}, \varphi) + b_n(Y^{h,U,+}_{ni} - Y^{h,U}_{ni}, \varphi) \\ =& \sum_{j=1}^{s} \bar{u}^0_{ij}(\sigma_n) b_n(Y^{h,+}_{n-1,j} - Y^h_{n-1,j}, \varphi) + \sum_{j=1}^{i-1} \bar{a}^0_{ij} b_n(E^{h,+}_{nj}, \varphi) \\ &+ \langle r_{ni}(Y^{h,+}_{n-1}, Y^h_n + E^{h,+}_n) - r_{ni}(Y^h_{n-1}, Y^h_n), \varphi \rangle. \end{aligned} \tag{26}$$

Note that $r_{ni}(Y_{n-1}^{h,+}, Y_n^h + E_n^{h,+})$ only depends on the first $i-1$ entries of $Y_n^h + E_n^{h,+}$. Especially it does not depend on $E_{ni}^{h,+}$.

Solving (26) for $E_{ni}^{h,+}$ on the whole space $\mathcal{V}_h^+$ is very expensive. To be more efficient, we only compute an error approximation $E_{ni}^{h,\oplus}$ on $\mathcal{V}_h^\oplus$ by solving

$$\begin{aligned} &\forall \varphi \in \mathcal{V}_h^\oplus : \\ b_n(E_{ni}^{h,\oplus}, \varphi) = &\sum_{j=1}^{s} \bar{u}_{ij}^0(\sigma_n) b_n(Y_{n-1,j}^{h,+} - Y_{n-1,j}^h, \varphi) + \sum_{j=1}^{i-1} \bar{a}_{ij}^0 b_n(E_{nj}^{h,\oplus}, \varphi) \\ &+ \langle r_{ni}(Y_{n-1}^{h,+}, Y_n^h + E_n^{h,\oplus}) - r_{ni}(Y_{n-1}^h, Y_n^h), \varphi \rangle. \end{aligned} \tag{27}$$

One can ask now, whether the approximation $E_{ni}^{h,\oplus}$ is reliable and efficient. We answer this question in the following Theorem 4.4. To this end, we further make the assumption that the strengthened Cauchy-Schwarz inequality holds.

Assumption 4.2 (Strengthened Cauchy-Schwarz Inequality)**.** There exists a constant $\delta \in [0, 1)$ independent of the finite element mesh $\mathfrak{T}$ and the time step size τ such that for the sesquilinear form (18) holds

$$|a_\tau(v, w)| \leq \delta ||v||_\tau ||w||_\tau \quad v \in \mathcal{V}_h, w \in \mathcal{V}_h^\oplus.$$

Then we cite the following Lemma from [2].

Lemma 4.2. *Let $\mathcal{V}_h^+ = \mathcal{V}_h \oplus \mathcal{V}_h^\oplus$ and $\bar{v} = \hat{v} + \check{v}$, where $\hat{v} \in \mathcal{V}_h$ and $\check{v} \in \mathcal{V}_h^\oplus$. Then the strengthened Cauchy-Schwarz inequality implies*

$$||\check{v}||_\tau \leq \frac{1}{\sqrt{1-\delta^2}} ||\bar{v} - v||_\tau \quad \forall v \in \mathcal{V}_h.$$

Furthermore, we have the following relation between $E_{ni}^{h,+}$ and $E_{ni}^{h,\oplus}$.

Lemma 4.3. *It holds for all $\varphi \in \mathcal{V}_h^\oplus$ that*

$$b_n(E_{ni}^{h,\oplus}, \varphi) = b_n(E_{ni}^{h,+}, \varphi) + \langle D_{ni}, \varphi \rangle \quad \text{for } i = 1, \ldots, s, \tag{28}$$

with D_{ni} defined by

$$D_{ni} = \sum_{j=1}^{i} \tilde{a}_{ij}^0 \left(r_{nj}(Y_{n-1}^{h,+}, Y_n^h + E_n^{h,\oplus}) - r_{nj}(Y_{n-1}^{h,+}, Y_n^h + E_n^{h,+}) \right),$$

$$\text{where } \tilde{a}_{ij}^0 = \begin{cases} 0 & \text{if } i = 1, \\ \sum_{l=j}^{i-1} \bar{a}_{il}^0 \tilde{a}_{lj}^0 & \text{if } j < i, \\ 1 & \text{if } j = i \text{ and } i > 1, \\ 0 & \text{if } j > i. \end{cases}.$$

Proof. Note that $r_{n1}(Y_{n-1}^{h,+}, Y_n^h + E_n^{h,+})$ and $r_{n1}(Y_{n-1}^{h,+}, Y_n^h + E_n^{h,\oplus})$ do not depend on any current stage values, hence we have

$$r_{n1}(Y_{n-1}^{h,+}, Y_n^h + E_n^{h,+}) = r_{n1}(Y_{n-1}^{h,+}, Y_n^h + E_n^{h,\oplus}).$$

We prove the Lemma by induction. Let $i = 1$. Then $\forall \varphi \in \mathcal{V}_h^{\oplus}$ it holds

$$\begin{aligned} b_n(E_{n1}^{h,\oplus}, \varphi) =& \sum_{j=1}^{s} \bar{u}_{1j}^0(\sigma_n) b_n(Y_{n-1,j}^{h,+} - Y_{n-1,j}^h, \varphi) \\ &+ \langle r_{n1}(Y_{n-1}^{h,+}, Y_n^h + E_n^{h,\oplus}) - r_{n1}(Y_{n-1}^h, Y_n^h), \varphi \rangle \\ =& \sum_{j=1}^{s} \bar{u}_{1j}^0(\sigma_n) b_n(Y_{n-1,j}^{h,+} - Y_{n-1,j}^h, \varphi) \\ &+ \langle r_{n1}(Y_{n-1}^{h,+}, Y_n^h + E_n^{h,+}) - r_{n1}(Y_{n-1}^h, Y_n^h), \varphi \rangle \\ =& b_n(E_{n1}^{h,+}, \varphi). \end{aligned}$$

Therefore $D_{n1} = 0$ for $i = 1$.

Now assume that the Lemma holds for some k. Then $\forall \varphi \in \mathcal{V}_h^{\oplus}$ we have

$$\begin{aligned} b_n(E_{n,k+1}^{h,\oplus}, \varphi) =& \sum_{j=1}^{s} \bar{u}_{k+1,j}^0(\sigma_n) b_n(Y_{n-1,j}^{h,+} - Y_{n-1,j}^h, \varphi) + \sum_{j=1}^{k} \bar{a}_{k+1,j}^0 b_n(E_{nj}^{h,\oplus}, \varphi) \\ &+ \langle r_{n,k+1}(Y_{n-1}^{h,+}, Y_n^h + E_n^{h,\oplus}) - r_{n,k+1}(Y_{n-1}^h, Y_n^h), \varphi \rangle \\ =& \sum_{j=1}^{s} \bar{u}_{k+1,j}^0(\sigma_n) b_n(Y_{n-1,j}^{h,+} - Y_{n-1,j}^h, \varphi) + \sum_{j=1}^{k} \bar{a}_{k+1,j}^0 b_n(E_{nj}^{h,+}, \varphi) \\ &+ \langle r_{n,k+1}(Y_{n-1}^{h,+}, Y_n^h + E_n^{h,+}) - r_{n,k+1}(Y_{n-1}^h, Y_n^h), \varphi \rangle \\ &+ \sum_{j=1}^{k} \bar{a}_{k+1,j}^0 \left\langle \sum_{l=1}^{j} \tilde{a}_{jl}^0 \Big(r_{nl}(Y_{n-1}^{h,+}, Y_n^h + E_n^{h,\oplus}) - \right. \\ &\qquad \left. r_{nl}(Y_{n-1}^{h,+}, Y_n^h + E_n^{h,+}) \Big), \varphi \right\rangle \\ &+ \langle r_{n,k+1}(Y_{n-1}^{h,+}, Y_n^h + E_n^{h,\oplus}) - r_{n,k+1}(Y_{n-1}^{h,+}, Y_n^h + E_n^{h,+}), \varphi \rangle. \end{aligned}$$

Hence we get $\forall \varphi \in \mathcal{V}_h^{\oplus}$

$$\begin{aligned} b_n(E_{n,k+1}^{h,\oplus}, \varphi) =& b_n(E_{n,k+1}^{h,+}, \varphi) \\ &+ \sum_{j=1}^{k+1} \tilde{a}_{k+1,j} \langle r_{nj}(Y_{n-1}^{h,+}, Y_n^h + E_n^{h,\oplus}) - r_{nj}(Y_{n-1}^{h,+}, Y_n^h + E_n^{h,+}), \varphi \rangle \\ =& b_n(E_{n,k+1}^{h,+}, \varphi) + \langle D_{n,k+1}, \varphi \rangle. \end{aligned}$$

We conclude that the Lemma holds also for $k + 1$. □

Using definition (25), we have the following splitting

$$D_{ni} = \tau_n D_{ni}^1 + D_{ni}^2 \tag{29}$$

with

$$\begin{aligned} D_{ni}^1 =& \gamma \sum_{k=1}^{i} \tilde{a}_{ik}^0 \Bigg(F\Big(t_{nk}, \sum_{j=1}^{s} \bar{u}_{kj}^0(\sigma_n) Y_{n-1,j}^{h,+} + \sum_{j=1}^{k-1} \bar{a}_{kj}^0 (Y_{nj}^h + E_{nj}^{h,\oplus})\Big) \\ &- F\Big(t_{nk}, \sum_{j=1}^{s} \bar{u}_{kj}^0(\sigma_n) Y_{n-1,j}^{h,+} + \sum_{j=1}^{k-1} \bar{a}_{kj}^0 (Y_{nj}^h + E_{nj}^{h,+})\Big) \Bigg). \end{aligned} \tag{30}$$

and

$$D_{ni}^2 = \sum_{k=1}^{i} \tilde{a}_{ik}^0 \sum_{j=1}^{k-1} (\bar{a}_{kj} - \bar{a}_{kj}^0)(E_{nj}^{h,\oplus} - E_{nj}^{h,+}). \tag{31}$$

The following theorem states that the error estimates $E_{ni}^{h,\oplus}$ are reliable and efficient up to some small perturbations.

Theorem 4.4. *Let $E_{ni}^{h,+} = \bar{E}_{ni}^h + \bar{E}_{ni}^{h,\oplus}$ where $\bar{E}_{ni}^h \in \mathcal{V}_h$ and $\bar{E}_{ni}^{h,\oplus} \in \mathcal{V}_h^{\oplus}$. D_{ni}^1 and D_{ni}^2 are given by equations* (30) *and* (31)*, respectively. Then we have*

$$\frac{\mu_b}{M_b} ||E_{ni}^{h,\oplus}||_\tau \leq (1+\beta)||E_{ni}^h||_\tau + \frac{1}{M_b}(\sqrt{\tau_n}||D_{ni}^1||_* + |D_{ni}^2|) \tag{32}$$

and

$$\begin{aligned}(1-\beta)\mu_b||E_{ni}^h||_\tau \leq & \frac{M_b}{\sqrt{1-\delta^2}}||E_{ni}^{h,\oplus}||_\tau + M_b||\bar{E}_{ni}^h||_\tau \\ & + \frac{1}{\sqrt{1-\delta^2}}(\sqrt{\tau_n}||D_{ni}^1||_* + |D_{ni}^2|).\end{aligned} \tag{33}$$

Proof. Using Lemma 4.3 for $\varphi = E_{ni}^{h,\oplus}$ and the ellipticity of the sesquilinear form $b_n(\cdot,\cdot)$ gives

$$\mu_b||E_{ni}^{h,\oplus}||_\tau^2 \leq b_n(E_{ni}^{h,\oplus}, E_{ni}^{h,\oplus}) = b_n(E_{ni}^{h,+}, E_{ni}^{h,\oplus}) + \langle D_{ni}, E_{ni}^{h,\oplus}\rangle.$$

It follows with the continuity of $b_n(\cdot,\cdot)$ and (29),

$$\mu_b||E_{ni}^{h,\oplus}||_\tau^2 \leq M_b||E_{ni}^{h,+}||_\tau||E_{ni}^{h,\oplus}||_\tau + (\sqrt{\tau_n}||D_{ni}^1||_* + |D_{ni}^2|)||E_{ni}^{h,\oplus}||_\tau.$$

Then the first inequality follows with (24).

To prove the second inequality we use the splitting $E_{ni}^{h,+} = \bar{E}_{ni}^h + \bar{E}_{ni}^{h,\oplus}$. We get, again using the ellipticity of $b_n(\cdot,\cdot)$, Lemma 4.3, and (29),

$$\begin{aligned}\mu_b||E_{ni}^{h,+}||_\tau^2 \leq & b_n(E_{ni}^{h,+}, E_{ni}^{h,+}) \\ = & b_n(E_{ni}^{h,+}, \bar{E}_{ni}^h) + b_n(E_{ni}^{h,+}, \bar{E}_{ni}^{h,\oplus}) \\ = & b_n(E_{ni}^{h,+}, \bar{E}_{ni}^h) + b_n(E_{ni}^{h,\oplus}, \bar{E}_{ni}^{h,\oplus}) - \langle D_{ni}, \bar{E}_{ni}^{h,\oplus}\rangle \\ \leq & M_b\left(||E_{ni}^{h,+}||_\tau||\bar{E}_{ni}^h||_\tau + ||E_{ni}^{h,\oplus}||_\tau||\bar{E}_{ni}^{h,\oplus}||_\tau\right) \\ & + (\sqrt{\tau_n}||D_{ni}^1||_* + |D_{ni}^2|)||\bar{E}_{ni}^{h,\oplus}||_\tau.\end{aligned}$$

Applying Lemma 4.2 with $v = 0$ gives

$$||\bar{E}_{ni}^{h,\oplus}||_\tau \leq \frac{1}{\sqrt{1-\delta^2}}||E_{ni}^{h,+}||_\tau.$$

Hence

$$\mu_b||E_{ni}^{h,+}||_\tau \leq \frac{M_b}{\sqrt{1-\delta^2}}||E_{ni}^{h,\oplus}||_\tau + M_b||\bar{E}_{ni}^h||_\tau + \frac{1}{\sqrt{1-\delta^2}}(\sqrt{\tau_n}||D_{ni}^1||_* + |D_{ni}^2|).$$

Finally (24) gives the second inequality. □

Remark 4.2. Let us briefly discuss the size of the perturbations on the right hand sides of the inequalities (32) and (33). Using Taylor expansion, condition (9), and the uniform boundedness of the operator A, we get $\sqrt{\tau_n}||D^1_{ni}||_* + |D^2_{ni}| \leq C_* \sum_{j=1}^{i-1} ||E^{h,+}_{nj} - E^{h,\oplus}_{nj}||_\tau$. Hence, the perturbations depend on the differences $E^{h,+}_{nj} - E^{h,\oplus}_{nj}$ and $E^{h,+}_{nj} - \bar{E}^h_{nj}$, which are in general of moderate size compared to the errors $E^{h,+}_{nj}$ and $E^{h,\oplus}_{nj}$ themselves. Alternatively, making use of $D^1_{n1} = D^2_{n1} = 0$, one could explore the estimator $E^{h,\oplus}_{n1}$ to design a spatial mesh for all stage values and hope that it is especially a good choice for Y_{ns}. □

To make the computation of the error estimation even more computationally efficient, we can replace $b_n(\cdot,\cdot)$ by an approximation $\tilde{b}_n(\cdot,\cdot)$ in (27). Then we get an approximation $\tilde{E}^{h,\oplus}_{ni}$ to $E^{h,\oplus}_{ni}$ by solving for all $\varphi \in \mathcal{V}^\oplus_h$:

$$\begin{aligned}\tilde{b}_n(\tilde{E}^{h,\oplus}_{ni}, \varphi) = &\sum_{j=1}^{s} \bar{u}^0_{ij}(\sigma_n) b_n(Y^{h,+}_{n-1,j} - Y^h_{n-1,j}, \varphi) + \sum_{j=1}^{i-1} \bar{a}^0_{ij} \tilde{b}_n(\tilde{E}^{h,\oplus}_{nj}, \varphi) \\ &+ \langle r_{ni}(Y^{h,+}_{n-1}, Y^h_n + \tilde{E}^{h,\oplus}_n) - r_{ni}(Y^h_{n-1}, Y^h_n), \varphi \rangle.\end{aligned} \tag{34}$$

Similar to Lemma 4.3 we have for all $\varphi \in \mathcal{V}^\oplus_h$ that

$$\begin{aligned}\tilde{b}_n(\tilde{E}^{h,\oplus}_{ni}, \varphi) &= b_n(E^{h,\oplus}_{ni}, \varphi) \\ &+ \left\langle \sum_{j=1}^{i} \tilde{a}^0_{ij} \left(r_{nj}(Y^{h,+}_{n-1}, Y^h_n + \tilde{E}^{h,\oplus}_n) - r_{nj}(Y^{h,+}_{n-1}, Y^h_n + E^{h,\oplus}_n) \right), \varphi \right\rangle\end{aligned} \tag{35}$$

with the same coefficients $\tilde{a}^0_{ij}$, $i,j = 1,\ldots,s$, as in Lemma 4.3. We get the following result concerning the relation between $\tilde{E}^{h,\oplus}_{ni}$ and $E^{h,\oplus}_{ni}$.

Theorem 4.5. *Assume that there are positive constants $\tilde{M}_b$ and $\tilde{\mu}_b$ such that the sesquilinear form $\tilde{b}_n(\cdot,\cdot)$ satisfies for all $v_1, v_2 \in \mathcal{V}^\oplus_h$*

$$|\tilde{b}_n(v_1, v_2)| \leq \tilde{M}_b ||v_1||_\tau ||v_2||_\tau, \tag{36}$$

$$\tilde{b}_n(v_1, v_1) \geq \tilde{\mu}_b ||v_1||^2_\tau. \tag{37}$$

Then

$$\frac{\tilde{\mu}_b}{M_b} ||\tilde{E}^{h,\oplus}_{ni}||_\tau \leq ||E^{h,\oplus}_{ni}||_\tau + \frac{\sqrt{\tau_n}||\tilde{D}^1_{ni}||_* + |\tilde{D}^2_{ni}|}{M_b}, \tag{38}$$

$$||E^{h,\oplus}_{ni}||_\tau \leq \frac{\tilde{M}_b}{\mu_b} ||\tilde{E}^{h,\oplus}_{ni}||_\tau + \frac{\sqrt{\tau_n}||\tilde{D}^1_{ni}||_* + |\tilde{D}^2_{ni}|}{\mu_b}, \tag{39}$$

with

$$\begin{aligned}\tilde{D}^1_{ni} = &\gamma \sum_{k=1}^{i} \tilde{a}^0_{ik} \Bigg(F\Big(t_{nk}, \sum_{j=1}^{s} \bar{u}^0_{kj}(\sigma_n) Y^{h,+}_{n-1,j} + \sum_{j=1}^{k-1} \bar{a}^0_{kj}(Y^h_{nj} + \tilde{E}^{h,\oplus}_{nj})\Big) \\ &- F\Big(t_{nk}, \sum_{j=1}^{s} \bar{u}^0_{kj}(\sigma_n) Y^{h,+}_{n-1,j} + \sum_{j=1}^{k-1} \bar{a}^0_{kj}(Y^h_{nj} + E^{h,\oplus}_{nj})\Big)\Bigg).\end{aligned}$$

and

$$\tilde{D}^2_{ni} = \sum_{k=1}^{i} \tilde{a}^0_{ik} \sum_{j=1}^{k-1} (\bar{a}_{kj} - \bar{a}^0_{kj})(\tilde{E}^{h,\oplus}_{nj} - E^{h,\oplus}_{nj}).$$

Proof. The inequalities follow similar to the proof of Theorem 4.4 using the relation (35) and the conditions (19), (20), and (36), (37). □

Remark 4.3. To approximate the sesquilinear form we use a diagonalization over $\mathcal{V}_h^{\oplus}$. Instead of one big global computation for $E_{ni}^{h,\oplus}$ we then can compute $\tilde{E}_{ni}^{h,\oplus}$ element-wise. For details we refer to [2, 11]. □

4.2.2. Implementation of the error estimator and mesh adaption

We have implemented the above described estimation process in KARDOS [3]. The error estimator $\tilde{E}_{ns}^{h,\oplus}$ for the last stage value $Y_{ns}^h \approx y(t_{ns})$ is used to drive the mesh adaptive approach along the main principle *Solve - Estimate - Refine - Solve*. After each succesfull timestep the mesh is coarsened before starting the next refinement, see [2] for details.

5. Time step control

When the multilevel finite element method successfully solved the spatial problem (14), the error in time has to be estimated and the time step size adapted. Following [1] and similar to Runge-Kutta methods we estimate the local error in time by comparing the computed solution approximation Y_{ns}^h at t_{n+1} to one of lower order. All considered linearly implicit peer methods have order $p = s - 1$ for variable step sizes. We compute an additional solution $\tilde{Y}_{ns}$ at time point t_{n+1} of order $\tilde{p} = s - 2$ as a combination of the approximations Y_{ni}^h, $i = 1, \ldots, s-1$. Hence we compute

$$\tilde{Y}_{ns} = \sum_{i=1}^{s-1} \alpha_i Y_{ni}^h. \tag{40}$$

For details on the computation of the coefficients α_i, $i = 1, \ldots, s-1$, we refer to [1]. An approximation of the local error in time is given by

$$\epsilon_n = Y_{ns}^h - \tilde{Y}_{ns}. \tag{41}$$

With m denoting the number of components of the PDE system (1) and the computed local temporal error approximation ϵ_n we define the following scaled scalar local error estimate

$$E_n^\tau := \left(\frac{1}{m} \sum_{i=1}^{m} \frac{||(\epsilon_n)_i||_{L_2}^2}{(ScalR_i \cdot ||(Y_{ns}^h)_i||_{L_2} + ScalA_i \cdot \sqrt{|\Omega|})^2} \right)^{\frac{1}{2}}$$

with user-prescribed relative and absolute scaling factors $ScalR_i$ and $ScalA_i$, respectively, for each component of the PDE system (1). If the computed E_n^τ is less than a tolerance TOL_t given by the user, the current step is accepted and otherwise rejected and repeated. In both cases, the step size for the next time step is defined as

$$\tau_{new} = \min \left\{ \tau_{max}, \min \left\{ \alpha_{max}, \max \left\{ \alpha_{min}, (TOL_t / E_n^\tau)^{1/(\tilde{p}+1)} \right\} \right\} \cdot \alpha_{safe} \cdot \tau_n \right\}.$$

For the parameters we set, c.f. [1],

$$\alpha_{min} = 0.2, \quad \alpha_{max} = 2, \quad \alpha_{safe} = 0.9.$$

The maximal step size τ_{max} is problem dependent.

To avoid unreasonable small last time steps, we follow the approach in [14]. Assume that the proposed step size is τ_{new}. To guarantee that we reach the endpoint T with a so-called averaged normal step length, we adjust τ_{new} to

$$\tau_{new} \leftarrow \frac{(T - t_n)}{\lfloor (1 + (T - t_n)/\tau_{new}) \rfloor}.$$

6. Efficiency of the spatial error estimator

A measure for the efficiency of the spatial error estimation at time point t_{ns} is the efficiency index

$$\mathrm{Eff}_n^{Space} := \frac{||\tilde{E}_{ns}^{h,\oplus}||_\tau}{||Y_{ns} - Y_{ns}^h||_\tau}. \tag{42}$$

In order to approximate the efficiency index, we perform one time step with the peer method on a fixed mesh and given exact initial values. The time step τ should not be too large, such that the time error does not dominate the spatial error. But it should also not be too small, such that the interpolation error of the initial values does not dominate. We compare then the computed solution with the exact solution. Since we only compute one time step, the global error is the same as the local error and the local spatial error estimation should be the same as the global error. Hence the efficiency index should be approximately one.

To demonstrate the quality of the hierarchical error estimator, we present the efficiency index for three test problems in 1D. In all computations we use a uniform mesh with n denoting the number of linear finite elements on the mesh.

1. **Linear problem.** This test problem is a heat equation with a linear source term. The domain is the unit interval $\Omega = (0, 1)$ and the equations are

$$\begin{aligned} \partial_t u - \partial_{xx} u &= u, \\ u(0, t) = u(1, t) &= 0, \\ u(x, 0) &= \sin(\pi x). \end{aligned} \tag{43}$$

   For this problem we have the following analytic solution:

$$u(x, t) = \exp((1 - \pi^2)t) \sin(\pi x).$$

2. **Ostermann's problem.** The following problem is taken from [5]. It is a heat equation with time-dependent source term on $\Omega = (0, 1)$ and reads

$$\begin{aligned} \partial_t u - \partial_{xx} u &= x \exp(-t), \\ u(0, t) = u(1, t) &= 0, \\ u(x, 0) &= \frac{1}{6} x(1 - x^2). \end{aligned} \tag{44}$$

   With the given initial condition, we have the following analytic solution:

$$u(x, t) = \left(\frac{\sin(x)}{\sin(1)} - x \right) \exp(-t).$$

n/τ	5.0000e−3	2.5000e−3	1.2500e−3	6.2500e−4
20	6.8326e−1	5.1968e−1	3.5143e−1	2.1334e−1
40	9.0108e−1	8.2037e−1	6.9575e−1	5.3364e−1
80	9.7399e−1	9.4937e−1	9.0373e−1	8.2447e−1
160	9.9348e−1	9.8702e−1	9.7438e−1	9.5007e−1

(a) Efficiency Index for the linear problem

n/τ	5.0000e−3	2.5000e−3	1.2500e−3	6.2500e−4
20	6.8485e−1	5.2084e−1	3.5217e−1	2.1374e−1
40	9.0156e−1	8.2081e−1	6.9613e−1	5.3391e−1
80	9.7408e−1	9.4949e−1	9.0385e−1	8.2458e−1
160	9.9347e−1	9.8704e−1	9.7441e−1	9.5010e−1

(b) Efficiency Index for Ostermann's problem

n/τ	1.2500e−3	6.2500e−4	3.1250e−4	1.5625e−4
160	5.1261e−1	3.4542e−1	2.0903e−1	1.1678e−1
320	8.0885e−1	6.7979e−1	5.1532e−1	3.4727e−1
640	9.4434e−1	8.9492e−1	8.1008e−1	6.8096e−1
1280	9.8543e−1	9.7152e−1	9.4471e−1	8.9529e−1

(c) Efficiency Index for the tanh problem

Table 1: Efficiency of the spatial error estimator

3. **Tanh problem.** This test problem is a heat equation on the domain $\Omega = (-3, 3)$ with nonlinear source term and no-flux boundary conditions given by

$$\begin{aligned} \partial_t u - \partial_{xx} u &= p_3(1-u^2) + 2p_2^2(u-u^3), \\ \partial_n u(-3,t) &= \partial_n u(3,t) = 0, \\ u(x,0) &= \tanh(p_2(x-p_1)). \end{aligned} \tag{45}$$

The problem is taken from [2] and was originally published in [15] to study moving-mesh strategies. The analytic solution is given by

$$u(x,t) = \tanh(p_2(x-p_1) + p_3 t).$$

We set $p_1 = 0.05$ and $p_2 = p_3 = 6.0$. Here, homogeneous Neumann boundary conditions are justified for small t.

In Table 1, the results for all test problems are shown. Starting at time point $t_0 = 0.01$ one time step with *peer4pos* for different mesh sizes n and different step sizes τ is computed. For fixed τ and increasing mesh size n, i.e. better spatial resolution, the efficiency index converges for all problems to the desired value one.

Note that the error estimator always underestimates the true global error. This stands in contrast to Rosenbrock solvers where it was observed, that the spatial error estimator tends to overestimate the spatial error [2].

7. Comparison of Peer-FE Methods with Rosenbrock-FE Methods

In this section we present a comparison of some Rosenbrock schemes and linearly implicit peer methods for two different test problems in 2D, see Sections

7.1 and 7.2. The Rosenbrock schemes used are the second order method *ros*2 [16], the third order method *ros*3*pl* [17], and the fourth order method *rodas*4*p* [18]. As stated in Section 3, the linearly implicit peer methods used are based on the coefficients of the singly implicit peer methods presented in [8]. These are the second order method *peer*3*pos*, the third order method *peer*4*pos*, and the fourth order method *peer*5*pos*.

The computations are all performed fully adaptive in time and space. The spatial tolerance TOL_x is always chosen equal to the time tolerance TOL_t, i.e. $TOL_x = TOL_t = TOL$. Several tests showed that this is usually a good choice with respect to accuracy and stability of the whole method.

7.1. Burgers problem

Our first test problem is the two dimensional Burgers equation [1],

$$\partial_t y_1 - \nabla \cdot (D \nabla u) = -a(y_1 \frac{\partial y_1}{\partial x_1} + y_2 \frac{\partial y_1}{\partial x_2}), \qquad \text{in } I \times \Omega, \tag{46}$$

$$\partial_t y_2 - \nabla \cdot (D \nabla v) = -a(y_1 \frac{\partial y_2}{\partial x_1} + y_2 \frac{\partial y_2}{\partial x_2}), \qquad \text{in } I \times \Omega. \tag{47}$$

Dirichlet and initial conditions are taken from the exact solution (48). The parameters are $D = 0.01$ and $a = 1$. The spatial domain is the unit square $\Omega = (0,1) \times (0,1)$ and the time interval is $I = [0,2]$. The exact solution is given by

$$\begin{aligned} y_1(x_1, x_2, t) &= \frac{3}{4} - \frac{1}{4a} \left(1 + \exp \frac{-4x_1 + 4x_2 - t}{32D} \right)^{-1}, \\ y_2(x_1, x_2, t) &= \frac{3}{4} + \frac{1}{4a} \left(1 + \exp \frac{-4x_1 + 4x_2 - t}{32D} \right)^{-1}. \end{aligned} \tag{48}$$

The exact solution depends in space only on the difference $x_1 - x_2$. Hence it is a wave starting at the diagonal $x_1 = x_2$ of the domain, and moving with a constant speed towards its north-west corner.

We approximate the exact $L_2(L_2)$ error in time and space by

$$||y_h - y||_{L_2(L_2)} \approx \left(\sum_{n=1}^{N} \tau_n ||Y_{ns}^h(\cdot) - y(\cdot, t_{ns})||_{L_2} \right)^{\frac{1}{2}}. \tag{49}$$

We have performed several runs with decreasing tolerance $TOL = 0.5^n \times 10^{-3}$, $n = 0, \ldots, 8$. In Figure 1 we see the $L_2(L_2)$ error of the computed approximation plotted over the computing time. The second order method *ros*2 is the least effective method with respect to achieved error versus computing time. The other methods tested are very similar in their performance. The fourth order methods *rodas*4*p* and *peer*5*pos* are slightly better than the third order methods *ros*3*pl* and *peer*4*pos*. As the wave moves with constant speed the time steps used are constant after a short initial phase. Since *peer*3*pos* is a third order method for constant time steps, it is no surprise that it shows a similar performance to *ros*3*pl*.

In Table 2a we give the number of time steps required for the different tolerance values. While the required number of time steps increases by a factor 17 for the finest tolerance compared to the coarsest tolerance for *ros*2, it only

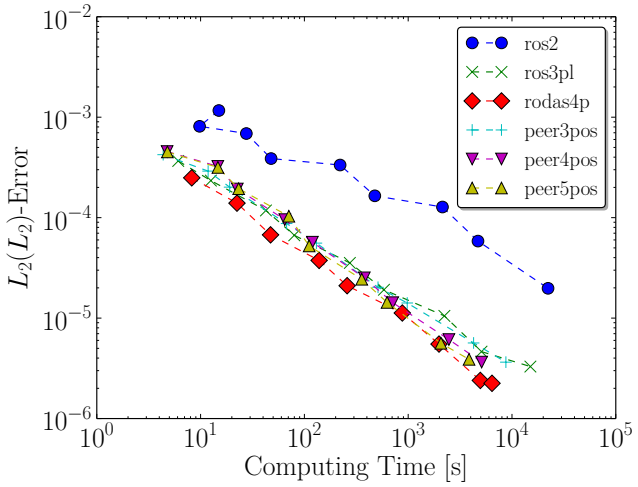

Figure 1: The $L_2(L_2)$-error plotted against the computing time for Burgers problem.

n/Method	ros2	ros3pl	rodas4p	peer3pos	peer4pos	peer5pos
0	37	20	17	18	17	15
1	53	23	18	22	21	20
2	76	28	20	26	24	21
3	108	34	23	33	27	24
4	155	41	25	42	30	25
5	218	51	28	54	35	27
6	309	63	31	71	41	29
7	436	81	35	94	47	32
8	615	104	39	127	56	34

(a) Number of time steps for a given local tolerance

n/Method	ros2	ros3pl	rodas4p	peer3pos	peer4pos	peer5pos
0	729	968	1088	729	729	729
1	754	1391	2398	1230	1249	1279
2	1201	2782	3709	1477	1536	1600
3	1456	4184	8592	3650	3666	3905
4	3634	11625	13973	4785	5091	5385
5	4876	16782	35826	13802	13157	14792
6	13644	46353	58730	17938	18996	20316
7	18524	70160	119783	51242	50484	58499
8	52705	147994	136896	70430	72998	78243

(b) Maximal number of spatial mesh points for a given local tolerance

Table 2: Number of time steps and maximal number of spatial mesh points for Burgers problem and tolerances $TOL = (0.5)^n \times 10^{-3}$.

doubles for *rodas4p* and *peer5pos*. For *peer4pos* it increases by a factor three, for *ros3pl* by a factor four, and for *peer3pos* by a factor five, respectively.

Finally in Table 2b we see the maximal number of spatial mesh points used for the given tolerance. During the integration with *ros2* the number of spatial nodes is much smaller than for the other methods. The integration with *rodas4p* uses the finest meshes. While the mesh sizes for the same spatial tolerance are similar for peer methods, they differ drastically for Rosenbrock methods.

7.2. Flame Problem

For the second test problem, we consider the propagation of a flame front through a cooled channel. This problem was published in [2] as a test problem for fully adaptive Rosenbrock-FE methods.

With a dimensionless temperature T, species concentration Y, and constant diffusion coefficients we look at the following system of equations

$$\begin{aligned} \partial_t T - \Delta T &= \omega(T,Y), && \text{in } \Omega \times (0,60], \\ \partial_t Y - \frac{1}{Le}\Delta Y &= -\omega(T,Y), && \text{in } \Omega \times (0,60], \\ T(\cdot,0) &= T_0(\cdot) && \text{on } \Omega, \\ Y(\cdot,0) &= Y_0(\cdot) && \text{on } \Omega. \end{aligned} \tag{50}$$

The Lewis number Le is the ratio of heat and mass diffusivity. The reaction is described by an Arrhenius law giving the following one-species reaction mechanism

$$\omega(T,Y) = \frac{\beta^2}{2Le} Y \exp\left(\frac{-\beta(1-T)}{1-\alpha(1-T)}\right). \tag{51}$$

The computational domain is a channel with width $H = 16$ and length $L = 60$. An obstacle with half of the width and length $L/4$ is positioned at $L/4$. The freely propagating laminar flame described by (50) is cooled at the obstacle. The heat absorption is modeled by a Robin boundary condition on $\partial\Omega_R$. On the left boundary of the domain, we prescribe Dirichlet conditions. The remaining boundary conditions are of homogeneous Neumann type. All this is represented by the following boundary conditions:

$$T = 1 \text{ on } \partial\Omega_D \times I, \quad \partial_n T = 0 \text{ on } \partial\Omega_N \times I, \quad \partial_n T = -\kappa T \text{ on } \partial\Omega_R \times I, \tag{52}$$

$$Y = 0 \text{ on } \partial\Omega_D \times I, \quad \partial_n Y = 0 \text{ on } \partial\Omega_N \times I, \quad \partial_n Y = 0 \text{ on } \partial\Omega_R \times I. \tag{53}$$

As initial condition we set

$$T_0(x) = \begin{cases} 1 & \text{for } x_1 \le x_0 \\ \exp(-(x - x_0)) & \text{for } x_1 > x_0 \end{cases}, \tag{54}$$

$$Y_0(x) = \begin{cases} 0 & \text{for } x_1 \le x_0 \\ 1 - \exp(-Le(x - x_0)) & \text{for } x_1 > x_0 \end{cases}. \tag{55}$$

The remaining parameters are chosen as

$$Le = 1, \quad \alpha = 0.8, \quad \kappa = 0.1, \quad \beta = 10, \quad x_0 = 9.$$

In Figure 2 the spatial meshes at time points $t = 20$ and $t = 40$ are shown for an integration with *peer4pos* and $TOL = 2.0 \times 10^{-4}$. The plots illustrate well the importance of spatial adaptivity for the flame problem. At $t = 20$ the flame is inside the channel and that is where most of the mesh refinement takes place. At $t = 40$ the flame has left the channel and now the mesh needs to be refined outside the channel, while inside the channel a coarser mesh is sufficient.

For this problem, we do not have an analytical solution. We computed a reference solution $\hat{y}$ at the time point T with $TOL = 10^{-5}$ using *ros3pl* and take the L_2-norm $||Y_{Ns}^h(\cdot) - \hat{y}(\cdot)||_{L_2}$ at time point $t_{end} = 60$ as numerical error.

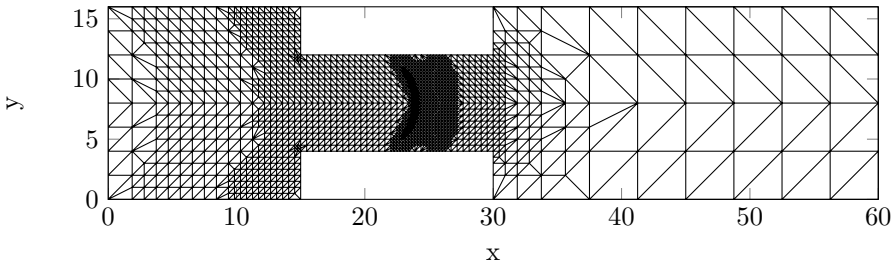

(a) Flame at time point $t = 20$.

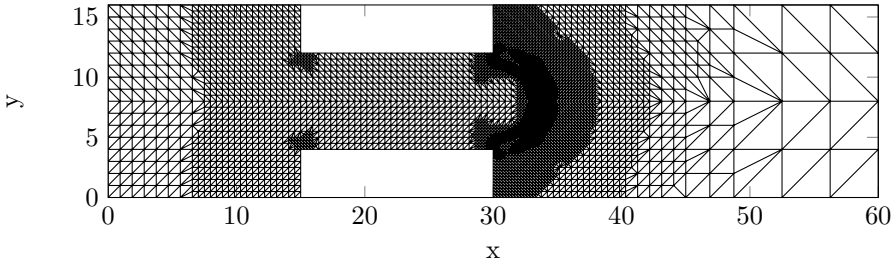

(b) Flame at time point $t = 40$.

Figure 2: Spatial meshes for the Flame problem within a integration with *peer4pos* and $TOL = 2.0 \times 10^{-4}$. Above at time point $t = 20$ the flame is inside the channel and in the figure below the flame already left the channel at time point $t = 40$.

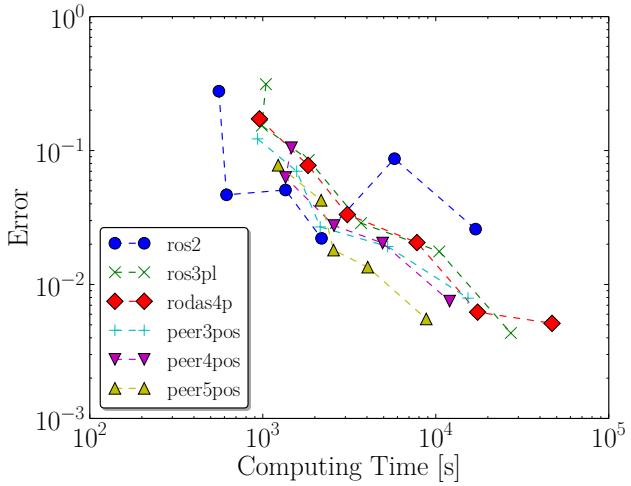

Figure 3: The numerical error $||Y^h_{Ns}(\cdot) - \hat{y}(\cdot)||_{L_2}$ at the final time point $t_{end} = 60$ plotted against the computing time for the flame problem.

We ran computations with different tolerances $TOL = 0.5^n \times 10^{-3}$, $n = 0, \ldots, 5$. For the coarsest tolerance $TOL = 10^{-3}$ the peer methods could not successfully compute a solution. For stricter tolerance values there were no difficulties. The performance of the methods is shown in Figure 3. With respect to the achieved error versus computing time *peer5pos* shows the best performance. The other methods, except *ros2*, have a similar performance, while *ros2* is again

n/Method	ros2	ros3pl	rodas4p	peer3pos	peer4pos	peer5pos
0	283	211	276	-	-	-
1	423	262	309	198	249	282
2	641	330	350	254	279	287
3	987	426	398	343	287	268
4	1501	551	456	472	360	282
5	2315	716	524	653	425	284

(a) Number of time steps for a given local tolerance

n/Method	ros2	ros3pl	rodas4p	peer3pos	peer4pos	peer5pos
0	546	1601	2516	-	-	-
1	932	3078	5514	2116	2281	2142
2	1815	6707	10962	3605	3658	3595
3	3357	12926	23836	7072	7204	7204
4	6959	28223	45196	13000	13377	13512
5	13370	52585	89514	27292	27397	27355

(b) Maximal number of spatial mesh points for a given local tolerance

Table 3: Number of time steps and maximal number of spatial mesh points for the flame problem and tolerances $TOL = 0.5^n \times 10^{-3}$.

the worst method.

In Table 3a the number of time steps used is shown. *peer5pos* needs the smallest number of time steps to satisfy the given error tolerance. Even for tighter tolerances the number of time steps used is only increasing a little. *rodas4p* and *peer4pos* need almost the same number of time steps for the same tolerance, while *ros3pl* needs the same number of time steps as *peer3pos*. This demonstrates the advantage of using time integrators not suffering from order reduction.

Again the maximal number of spatial mesh points needed differs a lot for Rosenbrock methods for a tolerance, while the peer methods require almost the same number of mesh points to fulfill a given tolerance, as can be seen in Table 3b.

8. Conclusion

In this paper we presented and analyzed a combination of linearly-implicit peer methods and multilevel finite element methods within a Rothe approach for parabolic problems. A spatial error estimator, based on the hierarchical basis approach, was derived and proven to be efficient and robust up to some small perturbations. These results for peer methods are similar to those for Rosenbrock methods employed in the same context. This led to a fully adaptive method for time-dependent PDEs.

In numerical experiments we could show the efficiency of the spatial error estimators for test problems in one spatial dimension. Furthermore we compared the performance of the fully adaptive linearly-implicit peer method to Rosenbrock methods for two test problems in two spatial dimensions. It could be seen that the linearly implicit peer methods based on coefficients taken from [8] are at least competitive with Rosenbrock methods for the test problems.

References

[1] A. Gerisch, J. Lang, H. Podhaisky, R. Weiner, High-order linearly implicit two-step peer - finite element methods for time-dependent PDEs, Applied Numerical Mathematics 59 (2009) 634–638.

[2] J. Lang, Adaptive Multilevel Solution of Nonlinear Parabolic PDE Systems - Theory, Algorithm, and Applications, Springer, Berlin, Heidelberg, 2001.

[3] B. Erdmann, J. Lang, R. Roitzsch, KARDOS-User's Guide, Manual, Konrad-Zuse-Zentrum Berlin (2002).
URL `https://opus4.kobv.de/opus4-zib/frontdoor/index/index/docId/709`

[4] B. Peth, Adaptive Two-Step Peer Methods for Incompressible Flow Problems, Verlag Dr. Hut, 2010.

[5] A. Ostermann, M. Roche, Rosenbrock methods for partial differential equations and fractional orders of convergence, SIAM Journal on Numerical Analysis 30 (4) (1993) 1084–1098.

[6] C. Lubich, A. Ostermann, Linearly implicit time discretization of non-linear parabolic equations, IMA Journal of Numerical Analysis 15 (4) (1995) 555–583.

[7] B. A. Schmitt, R. Weiner, Parallel two-step W-methods with peer variables, SIAM Journal on Numerical Analysis 42 (1) (2004) 265–282.

[8] S. Beck, R. Weiner, H. Podhaisky, B. A. Schmitt, Implicit peer methods for large stiff ODE systems, Journal of Applied Mathematics and Computing 38 (1-2) (2012) 389–406.

[9] C. L. Lawson, C^1-Compatible interpolation over a triangle, Technical Memorandum Jet Propulsion Labaratory (1976) 33–370.

[10] L. Petzold, Y. Cao, S. Li, R. Serban, Adaptive numerical methods for sensitivity analysis of differential-algebraic equations and partial differential equations, Workshop on Modelling and Simulation in Chemical Engineering, Coimbra, Portugal.

[11] P. Deuflhard, P. Leinen, H. Yserentant, Concepts of an adaptive hierarchical finite element code, IMPACT of Computing in Science and Engineering 1 (1) (1989) 3–35.

[12] P. Deuflhard, M. Weiser, Adaptive numerical solution of PDEs, Walter de Gruyter, 2012.

[13] W. Dörfler, R. H. Nochetto, Small data oscillation implies the saturation assumption, Numerische Mathematik 91 (1) (2002) 1–12.

[14] J. Lang, J. G. Verwer, On global error estimation and control for initial value problems, SIAM Journal on Scientific Computing 29 (4) (2007) 1460–1475.

[15] U. Nowak, Adaptive Linienmethoden für nichtlineare parabolische Systeme in einer Raumdimension, Ph.D. thesis, Freie Universiät Berlin (1993).

[16] J. G. Verwer, E. Spee, J. Blom, W. Hundsdorfer, A second-order Rosenbrock method applied to photochemical dispersion problems, SIAM Journal on Scientific Computing 20 (4) (1999) 1456–1480.

[17] J. Lang, D. Teleaga, Towards a fully space-time adaptive FEM for magnetoquasistatics, IEEE Transactions on Magnetics 44 (2008) 1238–124.

[18] G. Steinebach, Order reduction of row-methods for daes and method of lines applications, Tech. rep., Technische Hochschule Darmstadt (1995).